

## NUMERICAL INVESTIGATION OF TRANSIENT TEMPERATURE DISTRIBUTION IN ARC WELDING PROCESS

**Frank Webston Pontes dos Anjos<sup>a</sup>, frankwebston@hotmail.com**  
**Bruno Ramon Batista Fernandes<sup>b</sup>, brbfernandes@yahoo.com.br**

Federal University of Ceará, Fortaleza, Ceará, Brazil

<sup>b</sup>Department of Chemical Engineering

**José Robério de Castro Ferreira<sup>a</sup>, jr.ferreira@metalmat.ufc.br**

Federal University of Ceará, Fortaleza, Ceará, Brazil

**André Luiz Souza de Araújo, andre@ifce.edu.br**

Federal Institution of Ceará, Science and Technology of Ceará – IFCE

Industry Department

**Hélio Cordeiro de Miranda<sup>a</sup>, hmiranda@ufc.br**

Federal University of Ceará, Fortaleza, Ceará, Brazil

**Francisco Marcondes, marcondes@ufc.br**

Federal University of Ceará, Fortaleza, Ceará, Brazil

<sup>a</sup>Department of Metallurgical Engineering and Material Science

***Abstract.** Due to the high gradients along the welding parts, the heat transfer poses an overwhelming problem for the microstructures formed during the welding process. The heat transfer during the welding and pos-cooling process involve a phase change plus heat conduction in the areas around the welding zone, while the cooling process of welding parts involves natural convection and radiation. The way the work pieces are cooled affects the physical properties, microstructures, and residual stress distribution along the joint. The mathematical model to predict the temperature field in the welding parts can be based on the enthalpy method. The present paper shows a numerical and experimental evaluation of the temperature field in terms of welding cycles. Our main goal is to predict the microstructures formed during the cooling welding parts by comparing the CCT diagram with the experimental and numerical temperatures cycles. The present investigation takes into account the thermal conductivity variation with the temperature and considers a 3D temperature field.*

***Keywords:** Welding, Finite volume method, Heat transfer, Thermal cycle*

### 1. INTRODUCTION

Welding is a process of permanently union of materials through the action of interatomic and intermolecular forces that ensures the continuity of the material properties (Santos, 2001). Gas Tungsten Arc Welding (GTAW) is a process that melts and joins metal parts by heating them with an arc established between a non-consumable tungsten electrode and the metal parts. The understanding of this process turns possible the production of products with the appropriated mechanical characteristics. Several parameters affect the quality of welded materials such as, welding velocity, arc current, arc voltage, among them. Therefore, the correct choice of the welding parameters is crucial for the welding quality.

The literature presents some mathematical models devoted to the welding process, but they generally consider only two spacial dimensions, like the Rosenthal's analytical solution (Rosenthal, 1946). Yeh *et al* (2007) recently studied the problem using losses by natural convection, radiation and a distributed heat source, but the conductivity of the material was kept constant.

In the present work a three dimension mathematical model is employed. The input parameters are the welding parameters, plate dimensions, material and air properties. The output data are the temperature field and the welding cycles. The obtained welding cycles are also compared with experimental thermal cycles. In order to use the simulated results to predict the formed microstructures during the cooling process of the welding materials, the welding cycles are confronted with the material's Continuous Cooling Transformation diagram (CCT). Finally, a metallographic analysis of welding material is employed to check the results obtained in the previous analysis.

### 2. METHODOLOGY

The three dimensional, transient equation for the welding process in terms of enthalpy formulation (Özisk, 1993; Santos, 2001) is given by

$$\rho \frac{\partial H}{\partial t} = \nabla \cdot (K \nabla T) \quad (1)$$

where  $\rho$  is the density,  $H$  is the enthalpy,  $K$  is the thermal conductivity,  $T$  is the temperature and  $t$  is the time.

Equation (1) written for Cartesian system is given by

$$\rho \frac{\partial H}{\partial t} = \frac{\partial}{\partial x} \left( K \frac{\partial T}{\partial x} \right) + \frac{\partial}{\partial y} \left( K \frac{\partial T}{\partial y} \right) + \frac{\partial}{\partial z} \left( K \frac{\partial T}{\partial z} \right) \quad (2)$$

Figure 1 presents problem domain as well as the boundary conditions employed for the solution of Eq. (2).

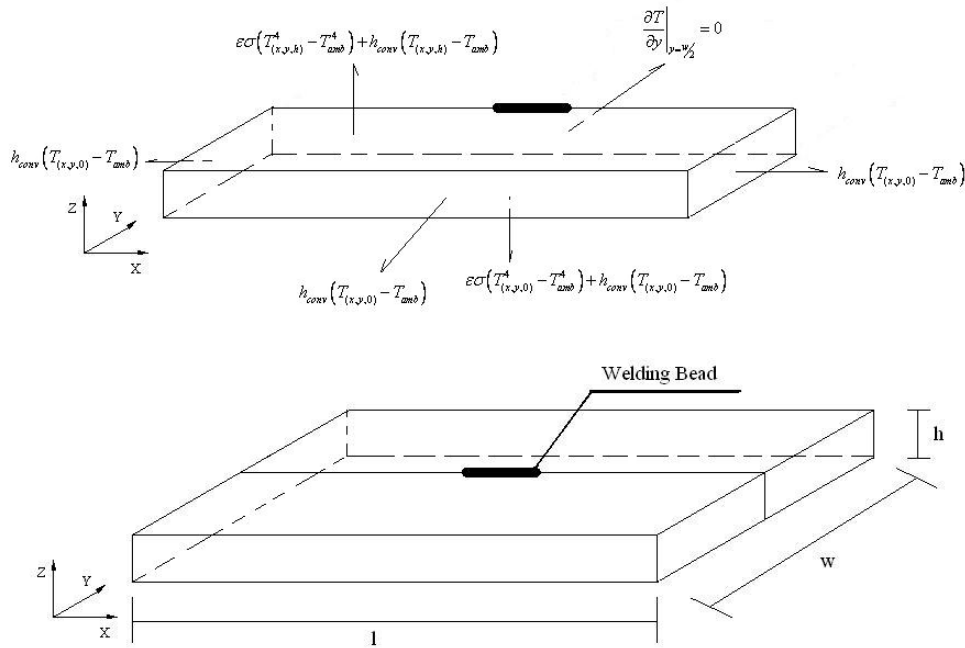


Figure 1. Illustration of the welded plate and boundary conditions.

Due to the symmetry of the problem along  $y$ , only the half of the shape was simulated. Therefore, as shown in Fig. 1, the boundary condition used along  $y = w/2$  is null flux. At  $z=0$  and  $z=h$  the following conditions that consider the losses by natural convection and radiation were used:

$$-K_p \frac{\partial T}{\partial z} \Big|_{z=0 \text{ or } z=h} = h(T_f - T_\infty) \quad (3)$$

where  $T_f$  denotes the temperature at  $z=0$  or  $z=h$  and  $K_p$  the thermal conductivity of the material measured at the ambient temperature. The convection coefficient along the upper and lower surface of the welding material is obtained from Incropera and Witt (1992).

$$Nu_L = \frac{h_L L}{k} = \begin{cases} 0,54 Ra_L^{1/4} \rightarrow \text{Hot surface and } Ra_L \leq 10^7 \\ 0,15 Ra_L^{1/3} \rightarrow \text{Hot surface and } Ra_L > 10^7 \\ 0,27 Ra_L^{1/4} \rightarrow \text{Cold Surface} \end{cases} \quad (4)$$

In Eq. (4)  $L$  is the characteristic length,  $k$  is the thermal conductivity of the fluid, and  $Ra_L$  is the Rayleigh number. The coefficient  $h_L$  is then summed up with the radiation heat transfer coefficient,  $h_r$ , generated from the linearization of the Boltzman's law equation of radiation.

$$h_r = \frac{\varepsilon\sigma(T_s^4 - T_\infty^4)}{T_s - T_\infty} \quad (5)$$

where  $\varepsilon$  is the emissivity of the material and  $\sigma$  the Boltzman's constant.

The other boundary conditions along the lateral surfaces have only convection and can be described by Eq. (3) as well. The  $h$ 's correlation for these bounds is described in Incropera and Witt (1992) to vertical walls.

Equation (2) is discretized through the finite-volume method. In this method the differential equation is integrated in the space according to Fig. 2 and time in order to have an approximated equation for each control volume.

$$\rho \left( \frac{H_p - H_p^0}{\Delta t} \right) \Delta V = K \left. \frac{\partial T}{\partial x} \right|_e \Delta y \Delta z - K \left. \frac{\partial T}{\partial x} \right|_w \Delta y \Delta z + K \left. \frac{\partial T}{\partial y} \right|_n \Delta x \Delta z - K \left. \frac{\partial T}{\partial y} \right|_s \Delta x \Delta z + K \left. \frac{\partial T}{\partial z} \right|_f \Delta x \Delta y - K \left. \frac{\partial T}{\partial z} \right|_b \Delta x \Delta y \quad (6)$$

where the superscript ' $\theta$ ' is defined in Eq. 7 (Maliska, 2004). For an explicit formulation, we have  $\theta=0$ , and  $\theta=1$  for a totally implicit formulation.

$$T^\theta = \theta T + (1-\theta)T^0 \quad (7)$$

In this work a fully implicit procedure was adopted. The derivatives in Eq. (6) were approached with the central difference scheme.

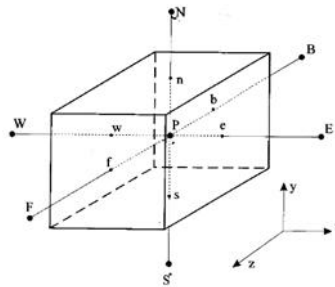


Figure 2. Control volume.

The thermal conductivity in each interface of the control volume was assumed to be a function of the temperature. The expression for  $K$  was presented by Özisik (1993).

$$K(T) = \begin{cases} \frac{T - T_0}{T_\gamma - T_0} (K_\gamma - K_0) + K_0 \rightarrow \text{If } T < T_{Ac} \\ K_\gamma \rightarrow \text{If } T_{Ac} \leq T < T_s \\ \frac{T - T_s}{\Delta T_{sl}} (K_l - K_\gamma) + K_\gamma \rightarrow \text{If } T_s \leq T < T_s + \Delta T_{sl} \\ K_l \rightarrow \text{If } T \geq T_s + \Delta T_{sl} \end{cases} \quad (8)$$

where the subscript ' $0$ ' denotes the terms related to the initial temperature or ambient temperature,  $K_\gamma$  denotes the thermal coefficient of the austenite,  $T_{Ac}$  denotes the austenite temperature,  $T_s$  denotes the steel melting temperature,  $K_l$  is the thermal conductivity of the steel in the liquid phase, and  $\Delta T_{sl}$  is the interval of temperature between the total solid phase and the total liquid phase.

On the other hand, the temperature is function of the enthalpy and can be defined, for a metal alloy (Özisik, 1993), by the following equation:

$$T(H) = \begin{cases} \frac{H}{C_p} \rightarrow \text{If } H < C_p T_s \\ \frac{H(T_l - T_s) + LT_s}{C_p(T_l - T_s) + L} \rightarrow \text{If } C_p T_s \leq H \leq (C_p T_l + L) \\ \frac{H - L}{C_p} \rightarrow \text{If } H > (C_p T_l + L) \end{cases} \quad (9)$$

where  $C_p$  is the thermal capacity of the alloy,  $L$  is the latent heat, and  $T_s$  and  $T_l$  are the total solid and liquid phase temperatures, respectively. This relationship allows us to replace the temperature by the enthalpy in Equations (1)-(8). This process gives rise to an implicit equation in terms of the enthalpy only.

For volumes along the superior surface ( $z=h$ ) and in contact with the welding arc, an additional heat must be considered, from the welding machine. In this work, we have used the expression given by Yeh *et al* (2007).

$$q = \frac{3\eta IU}{\pi\sigma_T^2} e^{\left(\frac{-3r^2}{\sigma_T^2}\right)} \Delta x \Delta y \quad (10)$$

where  $\eta$  is the welding process efficiency,  $r$  is the distance between the evaluated point to the center of the electrode,  $\sigma_T$  is the mean arc diameter,  $I$  is the electrode current and  $U$  is the voltage applied on the electrode.

The totally implicit formulation forms a non-linear system of equations, since the enthalpy of volume P and all neighborhood enthalpies at time level  $n+1$  need to be evaluated. For solving this system of equations, all the terms in Eq. (6) are placed on the same side of equation, and the temperatures are solved by Eq. (9), with estimated enthalpies. The other side of equation, that would be zero, is called residual function, and will have a value equals to zero, only when all enthalpies are solved. Replacing the temperatures in Eq. (6) and (9), and multiplying all the terms by  $\rho/\Delta t$ , the residual function for the volume  $i$  in the instant of time  $n+1$  is function of all enthalpies in the next time step, as showed in Eq. (11).

$$F_r(\vec{H}^{n+1})_i = H_i^n + \frac{\Delta t}{\rho} F(\vec{H}^{n+1})_i \quad (11)$$

As the function F showed in Eq. (11) is non-linear, the Newton-Raphson method is used to solve the system, calculating the derivatives of all residual functions numerically.

$$\frac{\partial F_r(\vec{H}^{n+1})_i}{\partial H_i^{n+1}} = \frac{F_r(\dots, H_{i-1}^{n+1}, H_i^{n+1} + \Delta H_i^{n+1}, H_{i+1}^{n+1}, \dots)_i - F_r(\dots, H_{i-1}^{n+1}, H_i^{n+1}, H_{i+1}^{n+1}, \dots)_i}{\Delta H_i^{n+1}} \quad (12)$$

The enthalpy of the next time step, in  $(k+1)$ -th iteration, is given by the addition of the enthalpy in the  $k$ -th iteration with the enthalpy variation that is calculated solving the system of equations linearized by the Newton-Raphson method.

The value of the enthalpy, in the first iteration, is estimated as the enthalpy of the previous time step, and the iteration process continues until each enthalpy variation ( $\Delta H$ ) reach the specified tolerance value.

In each iteration the linear system was solved using the algorithm BI -CGSTAB (van der Vorst, 1992) preconditioned at the right-hand side with an ILU factoring (Marcondes *et al*, 1995).

In the experiment, steel plates SAE 1045 were welded with a GTAW machine under welding conditions given in Tab. 1. The numerical conditions were the same as those used in the experiment. The employed thermophysical properties are summarized in Tab. 2.

Table 1. Welding process parameters.

Parameter	Value
Welding velocity(mm/s)	1
Weld bead length (mm)	100
Electrode current (A)	182.9
Electrode voltage (V)	11.6
Electrode diameter (mm)	1.6
Estimated arc diameter (mm)	13
Shape thickness (mm)	11
Process efficiency	75%
Distance between the electrode and the plate (mm)	3
Argon Flow Rate (min <sup>-1</sup> )	10
Electrode	2% ThO <sub>2</sub> -W alloy (EWTh-2)
Polarity	direct current electrode negative (DCEN)
electrode tip Angle	180 °

Table 2. Thermophysical properties used for the simulation.

	Properties	Value
Steel SAE 1045	L (J/Kg)	2.77·10 <sup>5</sup>
	K <sub>v</sub> (W/m/K)	30
	K <sub>l</sub> (W/m/K)	30
	K <sub>0</sub> (W/m/K)	60
	T <sub>0</sub> (K)	293.15
	T <sub>Ac</sub> (K)	1073.15
	T <sub>s</sub> (K)	1775.65
	T <sub>l</sub> (K)	1800.65
	ΔT <sub>sl</sub> (K)	25
	E	75%
Air	K (W/m/K) <sup>(1)</sup>	0.0462
	γ (K <sup>-1</sup> ) <sup>(1)</sup>	51·10 <sup>-6</sup>
	α (m <sup>2</sup> /s) <sup>(1)</sup>	72.1·10 <sup>-6</sup>

<sup>(1)</sup>: measured at 303K.

Three chromel–alumel K-type thermocouples wires of 1.5 mm diameter were used to get the welding cycles. The thermocouple junctions were soldered in the plate using a capacitive discharge device. Holes with 5 mm diameter were made on the opposite side of the plate to allow the temperature measurement inside the material. Figure 4 shows a schematic representation of the steel plate with 3 holes for fixing the thermocouple, as well the positions where the thermocouples were fixed.

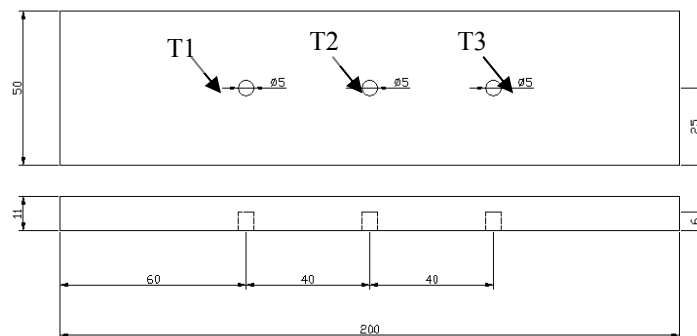


Figure 4. Schematic representation of used plate (dimensions, mm). T1 thermocouple near the begin of weld bead; T2 thermocouple at the middle of weld bead; T3 thermocouple near the end of weld bead.

All of the thermocouples were connected through coaxial cables to a data logger interfaced with a computer, and the temperature data were acquired automatically. A schematic representation of the experimental setup connected to the data acquisition and analysis system is shown in Fig. 5.

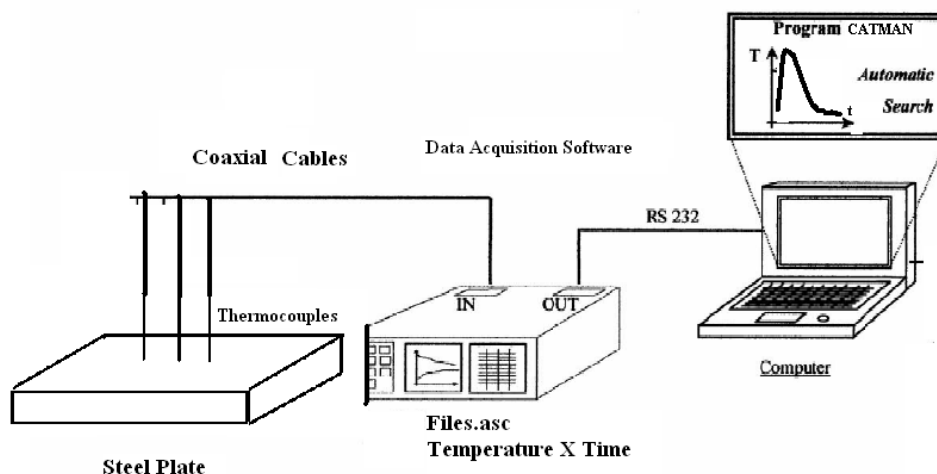


Figure 5. Schematic representation of the experimental setup.

For the investigation of the microstructure formed during the welding process of steel plate, samples from the welded plated were cut in the same approximated region where the thermocouples were placed and then metallographic techniques were applied for analyzing the microstructures formed in a optical microscopy (ASM International, 2004).

### 3. RESULTS AND DISCUSSION

In this section, numerical results from the simulations are presented. Also, the experimental welding cycles are compared with those obtained in the numerical simulations. Mesh refinement, close to the weld bead, in all three directions, were made in order to obtain a mesh-independent solution. Figure 6 presents the results of mesh refinement study, in terms of welding cycles, for thermocouples 1 and 2. From this figure, it is possible to observe that the difference between the mesh 75x51x23 and 101x61x27 are small. Therefore, the mesh presented in Fig. 7 was selected for all the numerical computations.

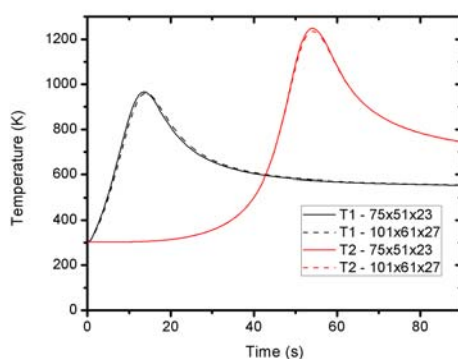


Figure 6. Mesh refinement study.

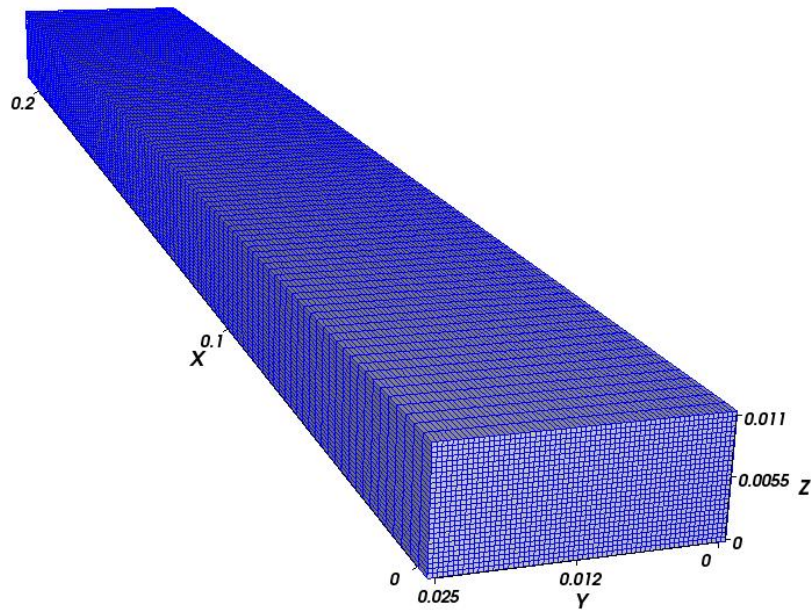


Figure 7. A 101x61x27 refined mesh.

Figure 8 present the temperature field in two simulation times. From the temperature field, shown in Fig. 8, it is possible to observe that the highest isotherm has the smallest radius of curvature, which is fully consistent with the warming process. Therefore, the higher temperature gradients are concentrated closer to the upper surface which is the region where the welding machine is located.

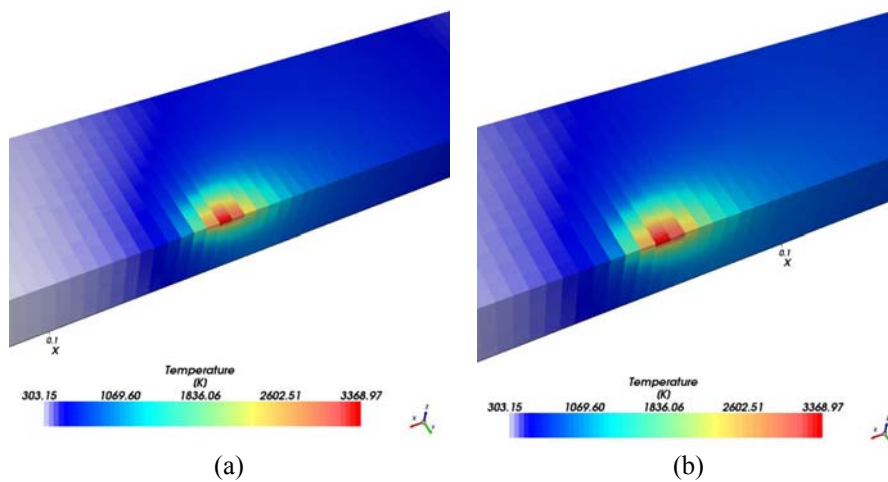


Figure 8. Transient temperature field. a) 54 seconds; b) 99 seconds.

In order to validate the numerical results the welding cycles were compared with the experimental cycles. Figure 9 shows the comparison between the experimental and the simulated results obtained for the T1 and T2 thermocouples. From the results presented in Fig. 9, we can observe that there are some differences between the experimental and numerical welding cycle curves close to the temperature peak. However, it should be emphasized that the region where the data set were obtained is very close to the weld bead, region where exist large uncertain in the parameters such as the maximum spread radius of the heat source, process efficient, among them.

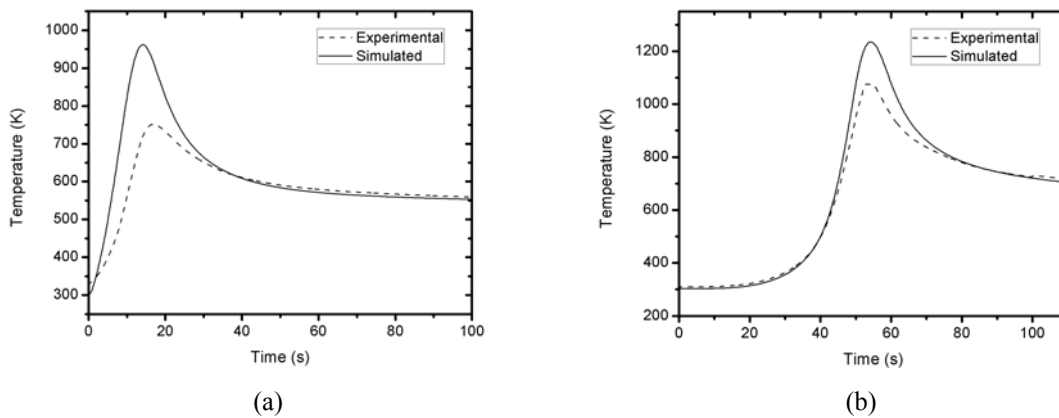


Figure 9. Experimental and simulated welding cycles. a)T1; b)T2.

Although differences between the experimental and simulated welding cycles were observed in Fig. 9, it is possible to verify the same trend in the numerical and experimental results during the cooling process. In fact, for the investigated material it is the cooling process that determines the mechanical properties of the welding process. For predicting the final microstructure of the material we choose, the CCT diagram of the steel SAE 1053 (NRIM-Special Report, 1999). This material was selected due to the similarity with the CCT Diagram of steel SAE 1045. Figure 10 shows the confrontation between the cooling curves of the experimental and simulated result for the T2 thermocouple, and the curves of the CCT diagram. From Figure 10, it is possible to observe that both numerical and experimental cooling curves predict that the weld bead will have only ferrite and pearlite as a final microstructure. This conclusion is supported by the metallographic analyze shown in Fig. 11.

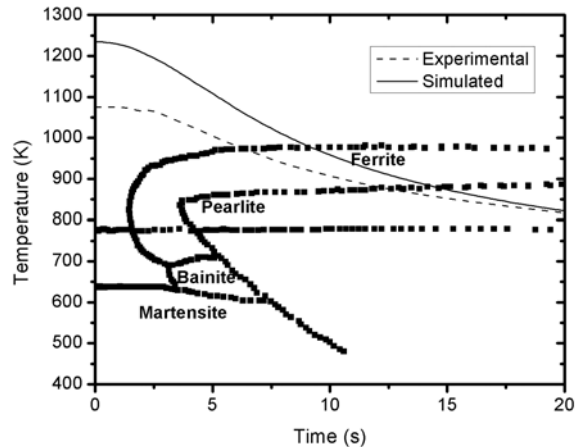


Figure 10. Comparison of experimental and simulated cooling curve, with the CCT Diagram. Adapted from NRIM-Special Report (1999).

Figure 11 presents the photomicrograph of the weld bead near T2 thermocouple. In this figure, the white grains denote the ferrite, and the dark grains denote the pearlite. The steel SAE 1045 is a transformable steel that can form martensite and bainite, which are microstructures susceptible to crack that decrease the material performance. The correct prediction of the formed microstructure during the welding process by the simulation can avoid the presence of undesirable microstructures.

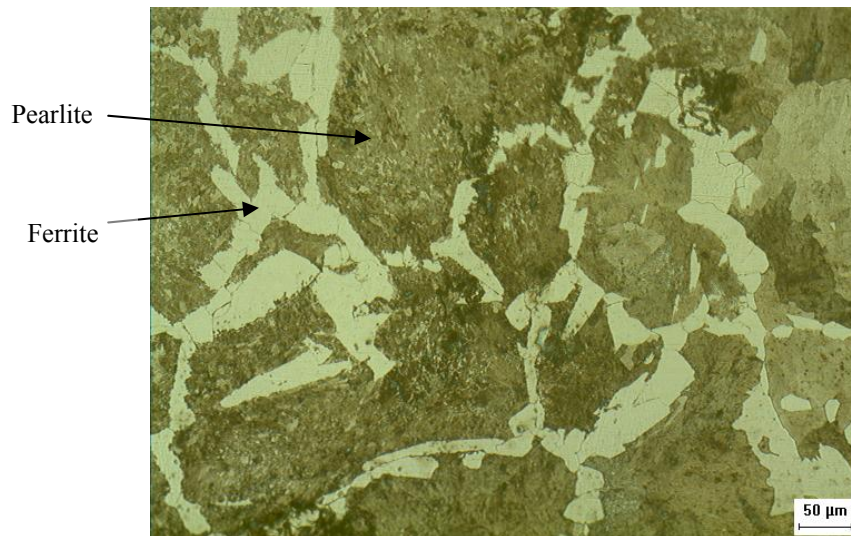


Figure 11. Photomicrograph of steel microstructure near to T2 thermocouple. 3% nital 200X. P - Pearlite (dark) and F - ferrite (white).

#### 4. CONCLUSION

The present paper presented the numerical and experimental results for the GTAW process. The 3D, transient heat conduction in terms of enthalpy were solved by the finite-volume method using a fully implicit procedure. Variation of thermal conductivity with temperature as well phase change during the welding process were taken into account. The model shows good results for predicting the microstructures formed due to the GTAW, which shows that this numerical tool can be used to predict the welding cycles and the microstructures formed in the welding process.

#### 5. ACKNOWLEDGEMENTS

The authors acknowledge the CNPQ and the Federal University of Ceará for the financial aid.

#### 6. REFERENCES

- ASM International, "ASM Handbook, Metallography and Microstructures", Materials Park, vol. 9, 2004.
- Incropera, F. P., Witt, D. P. Fundamentos de transferência de calor e de massa. 3<sup>a</sup>. Ed., LTC, Rio de Janeiro, Brasil, 1992.
- Maliska, C. R., "Transferência de Calor e Mecânica dos Fluidos Computacional", 2<sup>a</sup>. Ed., LTC, Rio de Janeiro, 2004.
- Marcondes, F., Zambaldi, M.C.; Maliska, C.R. "Comparação de Métodos Iterativos Não Estacionários em Malhas Não-Estruturadas de Voronoi na Solução de Problemas de Petróleo", XIII COBEM, Belo Horizonte, MG, Brasil, 1995.
- Nehad, A., "Enthalpy Technique for Solution Of Stefan Problems: Application To The Keyhole Plasma Arc Welding Process Involving Moving Heat Source", Int. Comm. HeatMass Transfer, Vol. 22, No. 6, pp. 779-790, 1995.
- NRIM, Special Report No. 99-02, 1999, "Atlas of CCT Diagrams for Welding (I)", National Research Institute for Metals, Edited by Takayoshi Kasugai and Mitsutane Fujita.
- Özisik, M. N., 1983, "Heat Conduction", 2nd Ed., Wiley.
- Rosenthal, D. "the Theory of Moving Source of Heat and Its Application to Metal Treatments", *Trats. ASME*, vol.68, pp. 849-866, 1946.
- Santos, L. A., 2001, "Heat Conduction in Welding with Thermal Pulsation", Ph.D. Dissertation, Universidade Federal de Santa Catarina. (in Portuguese).
- van der VORST, H. A. "BI-CGSTAB: a fast and smoothly converging variant of BI-CG for the solution of nonsymmetric linear systems", *SIAM Journal on Scientific and Statistical Computing*, vol. 13, No. 2, pp. 631-644, 1992.
- Yeh, R. H., Liaw, S. P., Tu, Y. P. "Transient Three-Dimensional Analysis of Gas Tungsten Arc Welding Plates. Numerical Heat Transfer, Part A: Applications", Vol. 51, No. 6, pp. 573-592, 2007.

#### 6. RESPONSIBILITY NOTICE

The authors are the only responsible for the printed material included in this paper.